ACS OMEGA

http://pubs.acs.org/journal/acsodf

Article

Strong Bathochromic Shift of Conjugated Polymer Nanowires Assembled with a Liquid Crystalline Alkyl Benzoic Acid via a Film Dispersion Process

Byoung Yun Jeon,[▽] Alemayehu Kidanemariam,[▽] Juran Noh, Chohee Hyun, Hyun Jung Mun, Kangho Park, Seung-Jin Jung, Yejee Jeon, Pil J. Yoo, JaeHong Park, Hee-Tae Jung, Tae Joo Shin,* and Juhyun Park*

Cite This: *ACS Omega* 2021, 6, 34876−34888

Read Online

ACCESS | Metrics & More | Article Recommendations | Supporting Information

ABSTRACT: We present aqueous dispersions of conjugated polymer nanowires (CPNWs) with improved light absorption properties aimed at aqueous-based applications. We assembled films of a donor−acceptor-type conjugated polymer and liquid crystalline 4-*n*-octylbenzoic acid by removing a cosolvent of their mixture solutions, followed by annealing of the films, and then formed aqueous-dispersed CPNWs with an aspect ratio >1000 by dispersing the films under ultrasonication at a basic pH. X-ray and spectroscopy studies showed that the polymer and liquid crystal molecules form independent domains in film assemblies and highly organized layer structures in CPNWs. Our ordered molecular assemblies in films and aqueous dispersions of CPNWs open up a new route to fabricate nanowires of low-band-gap linear conjugated polymers with the absorption maximum at 794 nm remarkably red-shifted from 666 nm of CPNWs prepared by an emulsion process. Our results suggest the presence of semicrystalline polymorphs β_1 and β_2 phases in CPNWs due to long-range $\pi-\pi$ stacking of conjugated backbones in compactly organized lamellar structures. The resulting delocalization with a reduced energy bang gap should be beneficial for enhancing charge transfer and energy-conversion efficiencies in aqueous-based applications such as photocatalysis.

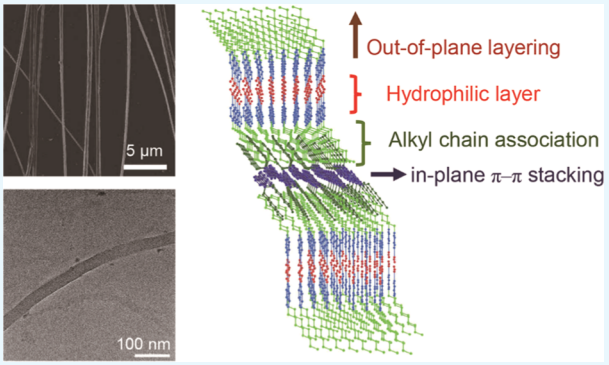

1. INTRODUCTION

Conjugated polymers are a popular material for optoelectronic,[1] biomedical,[2] and energy applications[3] because of their semiconducting properties and versatility in modulating their properties by adjusting their chemical structures. Through intra- and intermolecular charge transfer in assemblies of conjugated polymers, charge carriers can efficiently transport to enhance the efficiency of field-effect transistors (FETs),[4−6] light-emitting diodes (LEDs),[7−9] and photovoltaic cells.[10−12] In addition, they can efficiently harvest energy from a wide range of light, from ultraviolet (UV) to near-infrared (NIR) regions, by conveniently adjusting their band gaps, and either emit the energy as light or heat or transport it to other materials. Accordingly, they have been considered an ideal material for photoluminescence imaging[13−15] and sensing,[16−18] photoacoustic imaging[19−21] and photothermal therapy upon heat generation,[22−24] and photocatalysis reactions by efficient light harvesting.[3,25,26] The preparation of nanowires has been important for enhancing the performance in these applications. For example, charge transport efficiency in FETs can be significantly improved when conjugated backbones are assembled in one-dimensional (1D) nanowires, nanorods, or nanofibers due to the increased intermolecular charge transport.[27−29] In addition, intermolecular electron delocalization can narrow the band gaps of conjugated polymers, thereby enlarging the range of light absorption in the visible and NIR regions, thus enhancing light harvesting efficiency, which is useful when conjugated polymers are used as a photosensitizer in photocatalysis applications.[30−32]

Aqueous dispersions of conjugated polymer nanomaterials are particularly attractive in energy and environmental issues. As a photocatalyst or a photosensitizer combined with photocatalysts, conjugated polymer nanowires (CPNWs) can provide a useful method to harvest solar energy and utilize energy for photocatalysis reactions such as water splitting, hydrogen generation, and carbon dioxide conversion, and for degrading organic pollutants in aqueous media.[3,30] Charge

Received: October 6, 2021
Accepted: November 26, 2021
Published: December 6, 2021

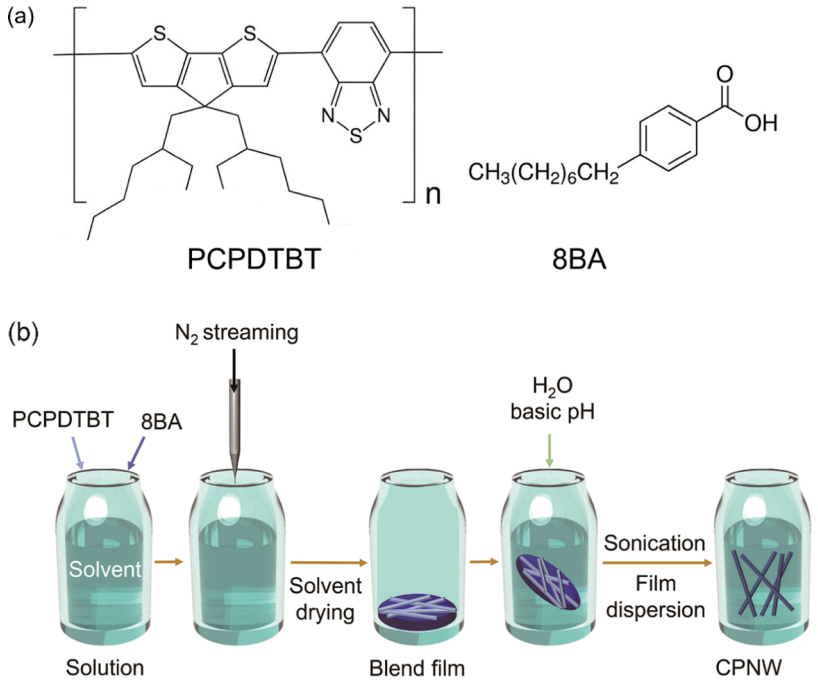

Figure 1. (a) Chemical structures of PCPDTBT and 8BA and (b) a schematic illustration of the overall assembly process.

transport along 1D assemblies can enhance the charge separation ability and increase the lifetime of a charge carrier when combined with other materials, resulting in increased photocatalytic activity. Although there are distinct advantages of CPNWs for energy harvesting and charge transport in such applications, fabricating 1D nanostructures of conjugated polymers in aqueous media has been challenging mainly because such aqueous dispersions of conjugated polymers typically require the use of amphiphiles that can partition the nanostructures of hydrophobic conjugated polymers and aqueous media at interfaces. Amphiphiles typically have alkyl tails and polar heads and are associated with conjugated polymers via lateral alkyl chain association, while 1D growth of CPNWs should occur by the $\pi-\pi$ stacking of conjugated backbones. In most cases, the lateral association and surface tension minimization at interfaces between conjugated polymers and aqueous media overwhelm intermolecular $\pi-\pi$ interactions between conjugated backbones, resulting in spherical morphologies.[33−35] Only a few studies have presented aqueous dispersions of CPNWs employing soft-templating[30] and emulsion processes.[36] In the in situ polymerization process using a mesophase as a soft template, monomers were confined to the cylindrical mesophase and converted to CPNWs by photoinitiated polymerization. The resultant CPNWs showed a significantly enhanced visible-light-active photocatalytic property.[30] In addition, we recently suggested the use of cylindrical alkyl benzoic acids as a soft template to guide the formation of CPNWs in an emulsification process.[36] However, it is difficult to form a closely packed structure of conjugated backbones via the emulsion process, which is indispensable for enhanced photophysical properties, and controlling molecular assemblies in 1D nanostructures of CPNWs remains challenging; thus, the development of new technologies is strongly required.

In this article, we present a method to prepare CPNWs as aqueous dispersions via the film assembly of a donor−acceptor-type conjugated polymer and liquid crystalline (LC) amphiphile, followed by a dispersion process of the film under ultrasonication. The donor−acceptor-type conjugated polymer, poly[2,6-(4,4-bis-(2-ethylhexyl)-4*H*-cyclopenta[2,1-*b*;3,4-*b*′]-dithiophene)-alt-4,7-(2,1,3-benzothiadiazole)] (PCPDTBT) can be assembled with 4-*n*-octylbenzoic acid (8BA), a representative nematic LC material, by hydrophobic associations between the ethylhexyl side chains of PCPDTBT and the octyls of 8BA due to its comparable length (Figure 1). Meanwhile, the hydrophilic carboxylic acids of 8BA can form acid dimers via hydrogen bonding and be separated from the remaining hydrophobic moieties, resulting in ordered film assemblies. Unlike the conventional emulsion process in which we used the same PCPDTBT and 8BA to prepare CPNWs,[36] the phase-separated film dispersion process takes advantage of ordered molecular structures in LC 8BA films to direct assemblies of CPNWs and via an annealing process to enhance their optical properties. As a characteristic of LC materials, 8BA can form crystalline structures in which the donor−acceptor-type amorphous conjugated polymer can be co-associated. We show that aqueous dispersions of PCPDTBT nanowires can be formed when water molecules penetrate the polar regions of the crystalline film assemblies of PCPDTBT and 8BA, thereby dispersing the films and resulting in CPNWs with an aspect ratio >1000 dispersed in aqueous media.

This article is organized as follows. We start with an analysis of thermal phase transitions, morphologies, and the formation of acid dimers in phase-separated films of PCPDTBT and 8BA assemblies compared to independent, pristine films of PCPDTBT and 8BA. The successful formation of CPNWs is demonstrated by preparing films at various molar mixing ratios of PCPDTBT to 8BA, followed by dispersing the films in basic conditions to break carboxylic acid dimers in the films. Our findings provide a basis for developing new CPNWs for aqueous-based applications including photoacoustic imaging, sensing, photothermal therapy, and photocatalysis.

https://doi.org/10.1021/acsomega.1c05556
ACS Omega 2021, 6, 34876−34888

2. RESULTS AND DISCUSSION

2.1. Film Assemblies of PCPDTBT and 8BA. The key to the preparation of aqueous-dispersed CPNWs via a film dispersion process is to take advantage of the ordered assemblies of a liquid crystalline alkyl benzoic acid when a donor−acceptor-type conjugated polymer is co-associated with the LC material. First, we investigated the phase transition behaviors of three films: 8BA, PCPDTBT, and assemblies of PCPDTBT/8BA at a 1:5 mixing ratio. These films were prepared by removing the cosolvent, toluene, from their solution mixtures by continuous, mild nitrogen blowing, and their thermal phase transition behaviors were monitored by differential scanning calorimetry (DSC).

The alkyl benzoic acid 8BA is a representative LC material that shows the phase transitions from a nematic to isotropic crystalline state upon increasing the temperature. Reportedly, 8BA shows three characteristic temperatures for crystal/crystal (T_{CC}), crystal/nematic (T_{CN}, melting of solid crystalline phases), and nematic/isotropic (T_{ISO}) phase transitions.[37] When the thermal phase transition behavior of 8BA was analyzed by DSC, it clearly presented T_{CC}, T_{CN}, and T_{ISO} at 31.63, 100.23, and 111.74 °C, by enthalpy changes of 27.18, 73.54, and 16.25 J g^{-1}, as shown in Figure 2. The polymorphic

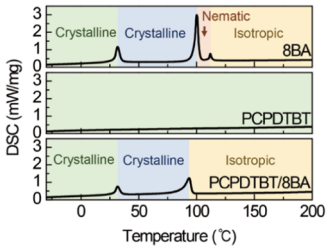

Figure 2. DSC thermograms of pristine 8BA, PCPDTBT, and PCPDTBT/8BA (1:5 molar mixing ratio) films.

melting transition below T_{CN} suggests a set of crystalline forms in the 8BA assembly. Obviously, three structural units of flexible aliphatic chains, stiff phenyl rings, and carboxylic acids contribute to the polymorphism in the 8BA assembly. In particular with numbers of methylene group higher than four for alkyl benzoic acids, the interactions between aliphatic chains and intrinsic conformational degrees of freedom significantly influence the molecular packing with the entropy increment per methylene group of 11 ± 1 J $(mol·K)^{-1}$ and possibly predetermine the formation of polymorphic crystalline forms, as investigated in the literature.[38] On the other hand, it is well known that the LC property of 8BA originates from hydrogen bonds and that the resultant formation of acid dimers hinders the complete melting of crystals to an isotropic state.[39] In comparison, the PCPDTBT film did not show any phase transition behavior (Figure 2) in the experiment window in our DSC study, indicating no phase transition. Meanwhile, the film assembly of PCPDTBT and 8BA at a 1:5 molar mixing ratio showed two peaks in its DSC thermogram (Figure 2), at 31.66 and 93.56 °C, by enthalpy changes of 7.16 and 61.35 J g^{-1}, respectively, which were transition temperatures close to T_{CC} and T_{CN} of the pristine 8BA. There was no transition peak around T_{ISO} of 8BA. These results indicate that the assembly of PCPDTBT and 8BA maintains crystalline molecular structures similar to those of 8BA, and the crystals melt at around 94 °C, which we denote as $T_{iso,mix}$ of the PCPDTBT/8BA assembly. The existence of a liquid crystalline phase in the PCPDTBT/8BA assembly was not detected, which could be clarified by temperature-dependent X-ray diffraction (XRD) measurements later.

Optical textures observed for films of 8BA and PCPDTBT/8BA assembly at a 1:5 mixing ratio show distinct variations near the transition temperatures measured by DSC, as shown in Figure 3a,b, respectively. Optical microscopy (OM) and polarized OM (POM) images of the 8BA film in Figure 3a show a crystalline texture up to 100 °C, the temperature around T_{CN}, and then the film is dewetted from the substrate surface after T_{CN} by melting the crystals into micro-droplets with a mesophase. In the droplets, the mesophase texture disappears at 115 °C beyond T_{ISO}, reappears at 110 °C upon cooling, and changes to a crystalline texture at 75 °C below T_{CN}. The optical textures of the PCPDTBT/8BA assembly at the 1:5 molar mixing ratio present an interesting morphological transition with increasing temperature. At 25 °C below T_{CC}, the film bears crystalline wires, as shown in the OM and POM images in Figure 3b; the wirelike crystalline structures disappear at 100 °C beyond $T_{iso,mix}$. Upon cooling, the wirelike crystalline structure is not recovered, and tiny crystals appear instead as shown in the OM and POM images below 90 °C (Figure 3b). Atomic force microscopy (AFM) analysis shows that the tiny crystals have a nanorod-like morphology, as shown in Figure 4. AFM images scanned in a height mode clearly show long wires before thermal treatment (Figure 4a) and rod-like morphology about 120 nm in length and 70 nm in width after thermal annealing (Figure 4b). These results show that PCPDTBT chains form a wirelike crystalline structure by assembling with 8BA LC molecules upon solvent drying. Wire morphology is transformed to nanorod morphology with heat treatment by surface-free-energy minimization upon melting of 8BA in the PCPDTBT/8BA assembly.

To elucidate the morphological changes with phase transitions, we analyzed the FT-IR spectra of three films. The Fourier transform infrared (FT-IR) spectrum of 8BA without thermal treatment in Figure 5a shows characteristic bands for O−H stretching (an amorphous hollow at 3300−2500 cm^{-1}) with Fermi resonance coupling (2669.5 and 2549.0 cm^{-1}), aromatic and aliphatic C−H stretching (3200−2800 cm^{-1}), asymmetric C═O stretching (1678.3 cm^{-1}), aromatic C═C stretching (1600−1400 cm^{-1}), C−O stretching (1290.2 cm^{-1}), and out-of-plane O−H bending (941.6 cm^{-1}). The band positions of carbonyl stretching in the 8BA film are characteristic for closed dimers of aryl acids,[38,40] proving that hydrogen bonds form in the 8BA film. Also, the strong, broad O−H stretching band extended from 2500 to 3300 cm^{-1}, which are overlapped with sharp C−H stretching peaks, is indicative of the existence of hydrogen-bonded acid dimers.[38] The FT-IR spectrum of the PCPDTBT film in Figure 5a presents characteristic peaks for aromatic and aliphatic C−H stretching (3200−2800 cm^{-1}) and aromatic ring stretching (1600−1300 cm^{-1}). The characteristic ring stretching peaks of thiophene and cyclopentadiene in PCPDTBT are indicated by red arrows at 1504.2 and 1396.2 cm^{-1} (Figure 5a), respectively, which are coincident with the literature.[41] Notably, the characteristic peaks for closed acid dimers, thiophene, and cyclopentadiene also appear in the FT-IR spectrum of PDPCTBT/8BA film as shown in Figure 5a. They are the OH stretching band (3300−2500 cm^{-1}), the carbonyl stretching band (1678.8 cm^{-1}), and ring stretching bands of thiophene and cyclopentadiene (1504.2 and 1397.2

https://doi.org/10.1021/acsomega.1c05556
ACS Omega 2021, 6, 34876−34888

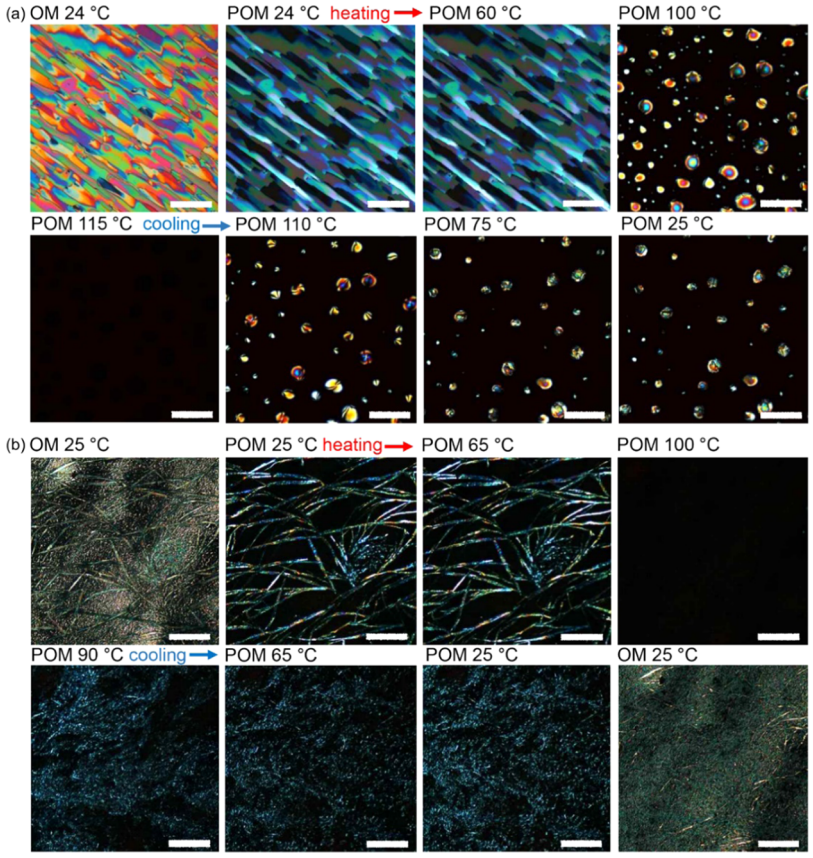

Figure 3. Optical textures of (a) 8BA and (b) PCPDTBT/8BA (1:5 molar mixing ratio) films with heating and cooling. Scale bars are 100 μm.

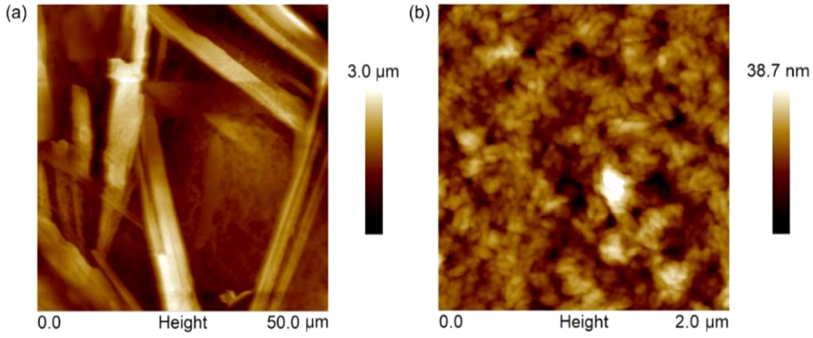

Figure 4. AFM images of PCPDTBT/8BA (1:5 molar mixing ratio) films at room temperature (a) before and (b) after heat treatment.

cm^{-1}). These results clearly indicate that 8BA molecules do form closed dimers of acyl acids via hydrogen bonding after assembling with PCPDTBT in the film and suggest that 8BA molecules might form crystal structures in assembly with PCPDTBT.

In situ FT-IR study of the PCPDTBT/8BA film assembled at a 1:5 molar mixing ratio film reveals the origination of $T_{iso,mix}$. The strong, broad OH stretching band clearly shown at 25 °C in Figure 5b disappears above 100 °C. Also, the strong carbonyl stretching band characteristic for aryl acid dimers at 1678.8 cm^{-1} at 25 °C also disappears above 100 °C, and acid monomer bands at around 1730 and 1718 cm^{-1} only remain. These results indicate that $T_{iso,mix}$ is the temperature at which hydrogen bonds between aryl acids are broken and free acid monomers are formed.

The temperature-dependent XRD measurements in Figure 6 clearly show the crystallographic evolution corresponding to phase transitions confirmed by DSC thermograms and in situ FT-IR spectra. The XRD pattern of 8BA powder (Figure 6a) measured in a capillary tube clearly shows a triclinic structure at room temperature (space group $P1$, a = 13.64 Å, b = 21.92 Å, and c = 7.64 Å; α = 90.02°, β = 101.05°, γ = 108.02° at 20 °C; see Figure S1 and Table S1 for a representative Rietveld analysis of XRD data based on a whole-pattern profile matching method using the FullProf Suite and temperature-dependent analysis results, respectively). This crystal structure is transformed into the same triclinic structure of the identical crystal phase with different lattice constants and angles above T_{CC} ($P1$, a = 13.50 Å, b = 22.79 Å, and c = 7.59 Å; α = 98.37°, β = 99.55°, γ = 101.43° at 60 °C) and a mixture of a mesophase and the crystal phase near T_{CN} ($P1$, a = 9.74 Å, b = 21.11 Å, and c = 7.68 Å; α = 92.65°, β = 103.70°, γ = 93.71°; $P1$, a = 13.56 Å, b = 23.05 Å, and c = 7.60 Å; α = 99.90°, β = 99.08°, γ = 100.46° at 95 °C), single mesophase above T_{CN}

https://doi.org/10.1021/acsomega.1c05556
ACS Omega 2021, 6, 34876−34888

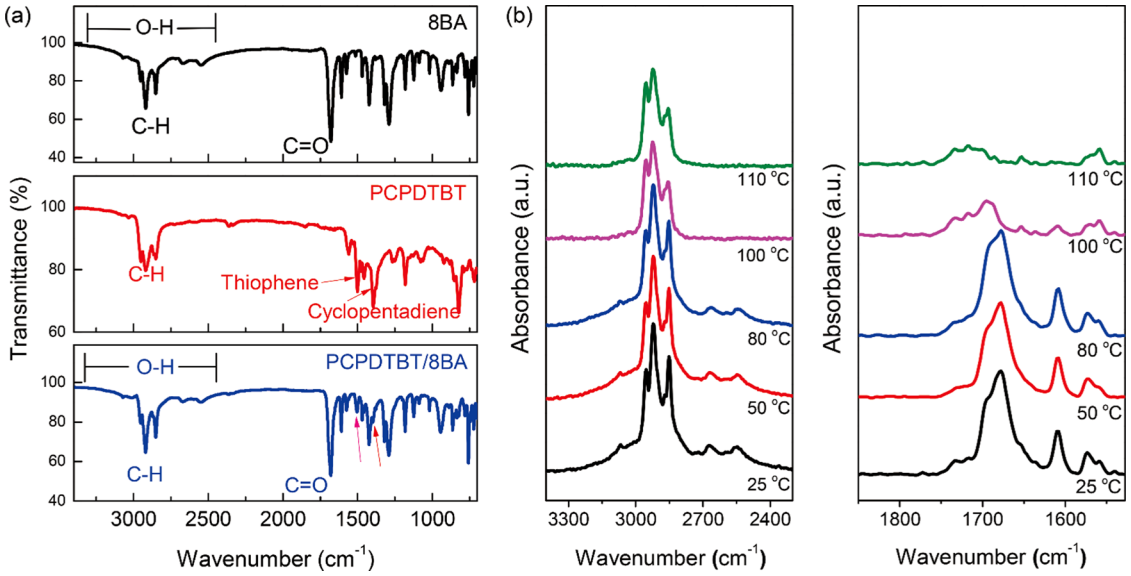

Figure 5. (a) FT-IR spectra of pristine 8BA, PCPDTBT, and PCPDTBT/8BA (1:5 molar mixing ratio) films at room temperature before heat treatment. (b) In situ FT-IR spectra of PCPDTBT/8BA (1:5 molar mixing ratio) film with temperature change to monitor O−H stretching with Fermi resonance coupling and carbonyl stretching bands.

($P1$, a = 9.74 Å, b = 21.13 Å, and c = 7.66 Å; α = 92.56°, β = 103.93°, γ = 93.79° at 105 °C) and disappears after T_{iso}.

In comparison, PCPDTBT scraped up from its film formed in a vial by solvent drying with nitrogen blowing did not show distinct crystal peaks in its XRD pattern (Figure 6b). It showed only three blunt diffraction peaks at around q = 0.598, 1.064, and 1.540 Å^{-1}, respectively. These peak positions correspond to those of the (110), (130), and (150) planes in an orthorhombic cell of crystalline PCPDTBT[42,43] and did not change with an increase in temperature, indicating that there was a slight ordering and not a crystalline structure, and showed no structural variation up to 150 °C.

In the XRD pattern of the PCPDTBT/8BA assembly (Figure 6c), characteristic diffraction peaks for both 8BA and PCPDTBT appeared simultaneously. Interestingly, the temperature-dependent lattice constants and angles of the crystal structure in the PCPDTBT/8BA assembly at a 1:5 molar mixing ratio presented in Figure 6f,g are almost coincident with those of the pristine 8BA as shown in Figure 6d,e. The XRD pattern of PCPDTBT/8BA shows a triclinic structure at 20 °C (space group $P1$, a = 13.64 Å, b = 21.72 Å, and c = 7.63 Å; α = 89.38°, β = 101.08°, γ = 107.03°). This crystal structure is transformed into the same triclinic structure of the identical crystal phase with different lattice constants and angles above T_{CC} ($P1$, a = 13.51 Å, b = 22.84 Å, and c = 7.61 Å; α = 98.08°, β = 99.37°, γ = 101.30° at 60 °C). A mixture of a mesophase and the crystal phase appears near 95 °C ($P1$, a = 9.73 Å, b = 21.12 Å, and c = 7.65 Å; α = 92.56°, β = 103.36°, γ = 93.74°; $P1$, a = 13.58 Å, b = 23.18 Å, and c = 7.58 Å; α = 100.20°, β = 98.43°, γ = 101.13° at 95 °C), and disappears above 95 °C. These results mean that 8BA and PCPDTBT exist as independent regions in the assembly of PCPDTBT and 8BA. Figure 6c looks almost like a superposition of Figure 6a,b, suggesting that the PCPDTBT/8BA assembly is a simple phase-separated blend of the pure polymer and pure 8BA. The differences in DSC transition temperatures can be attributed to finite size effects due to the existence of PCPDTBT domains in the excess 8BA domains in the film of the PCPDTBT/8BA assembly. Because more 8BA than PCPDTBT was used, it is plausible that PCPDTBT chains are associated with 8BA at the outmost surface of 8BA crystal domains and that the domains of PCPDTBT are inserted in the alkyl chain regions in between the 8BA crystal domains.

Both the DSC and temperature-dependent XRD results present decreases in energies required for melting transitions, T_{CN} and T_{iso}, when PCPDTBT molecules are assembled with 8BA, indicating that the association between PCPDTBT and 8BA disrupts the original crystal structure of 8BA. Pristine 8BA assembly has three regions of alkyl chain packing, $\pi-\pi$ stacking between phenyl rings, and hydrogen bonding between carboxylic acids, as described in studies regarding alkyl benzoic acids.[44] Three phase transition temperatures of T_{CC}, T_{CN}, and T_{iso} should be related to order/disorder transitions of three structural elements in 8BA. The melting enthalpy at T_{CC} significantly decreased, from 31.63 to 7.16 J g^{-1}, although the peak position for the melting transition is the same, at 31.6 °C. The melting enthalpies at T_{CN} and T_{iso} also decreased from 89.79 to 61.35 J g^{-1}. The transition temperatures, T_{CN} and T_{iso}, subsequently decreased and merged from 100.23 and 111.74 to 93.56 °C, showing the influence of the finite size effect by blending the PCPDTBT domains in the 8BA assembly.

With the DSC, XRD, and in situ FT-IR results, the crystal structure of wires shown in POM and AFM images (Figures 3b and 4a) measured before thermal treatment provides us a motif of the PCPDTBT and 8BA assembly. The (150) plane shown in Figure 6b is a characteristic diffraction peak by $\pi-\pi$ stacking of conjugated planes in the PCPDTBT assembly. Thus, it is also plausible that PCPDTBT chains are self-associated with each other via the $\pi-\pi$ stacking forming their independent regions and that their alkyl side chains are associated with octyls of 8BA between 8BA crystal domains, forming the wirelike morphology before the heat treatment. It seems that the wirelike morphology is not in the thermodynamically most stable state, mainly because the assembly film is prepared by evaporating the solvent with nitrogen gas blowing. The long-wire-like morphology was transformed to the film with a fine texture upon heating by surface energy minimization above

https://doi.org/10.1021/acsomega.1c05556
ACS Omega 2021, 6, 34876−34888

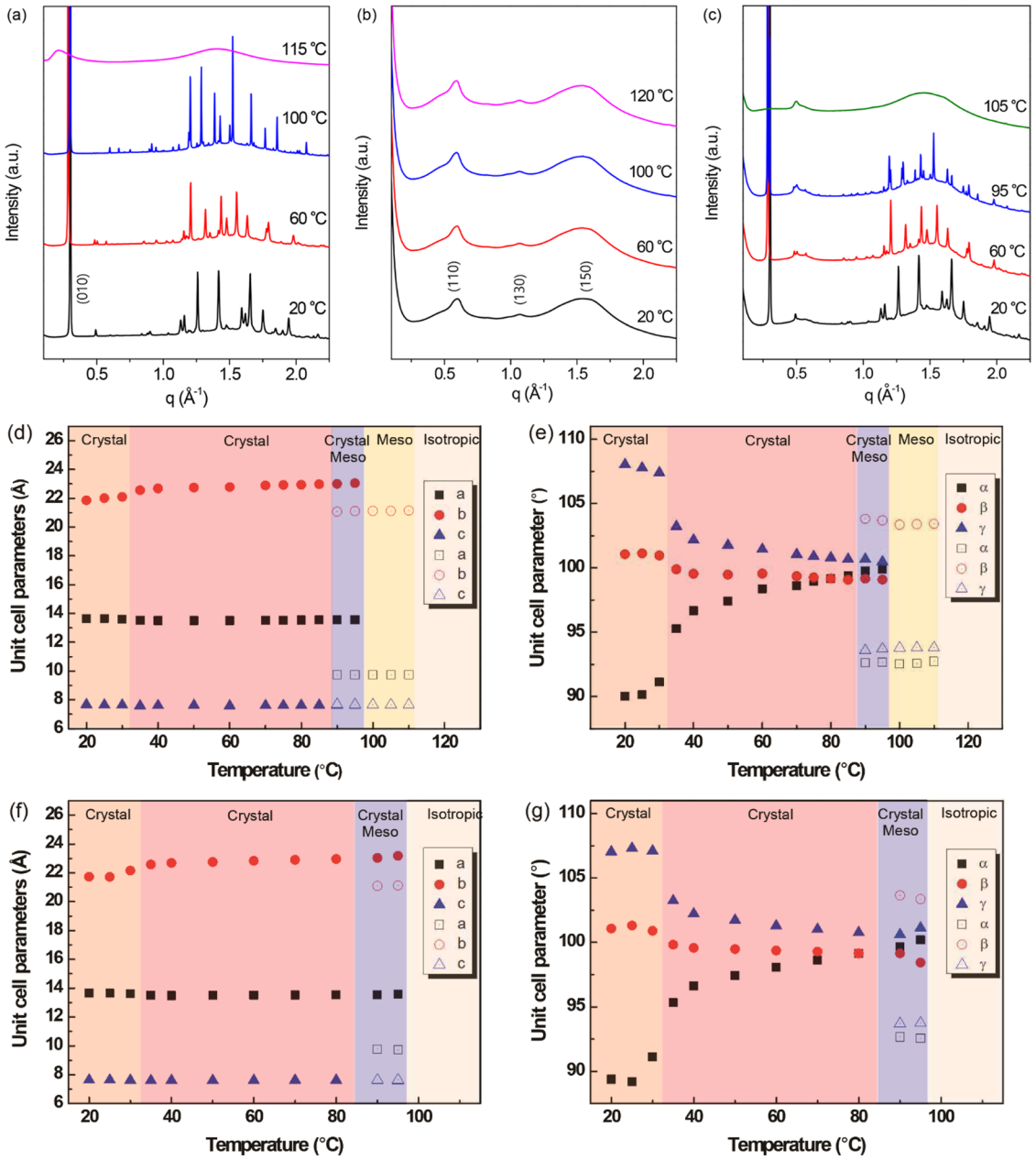

Figure 6. Temperature-dependent XRD patterns of (a) pristine 8BA, (b) PCPDTBT, and (c) PCPDTBT/8BA assembly at a molar mixing ratio of 1:5. Temperature-dependent lattice constants and angles of (d, e) pristine 8BA and (f, g) PCPDTBT/8BA assembly, respectively.

$T_{iso,mix}$, where the 8BA crystal melted and hydrogen bonds between aryl acids are broken (Figures 3b and 4b).

2.2. CPNWs of PCPDTBT and 8BA. The film assemblies of PCPDTBT and 8BA were dispersed in basic aqueous solutions under ultrasonication to form CPNWs. An optimal basic condition was required to obtain CPNWs that were independently dispersed with a narrow width of less than one micrometer. The concentration of 8BA in 2 mL of aqueous solution that contained PCPDTBT/8BA assembly at a 1:5 molar mixing ratio was 0.935 mM. After adding aqueous solutions at pHs 10, 11, 12, 13, and 14 followed by ultrasonication, the pHs of the resulting solutions were changed to 5.61, 6.24, 7.09, 9.71, and 12.46, respectively. With these concentrations of [H+] and pK_a values of benzoic acid (pK_a = 4.2),[45] the % degrees of ionization are estimated to be substantially high enough for dispersing CPNWs by electrostatic repulsion of carboxylate ions. Interestingly, a successful dispersing of the assembly occurred at pH 12, where the concentration of hydroxyl ion [OH−] was 1 mM. When the pHs of aqueous solutions that were added into vials with dry PCPDTBT/8BA assemblies were 10 and 11, micrometer-scale rods were shown after ultrasonication, indicating that the film dispersing into nanowires is inefficient (Figure S2a and S2b). At pHs 13 and 14, there exist significantly excessive amounts of NaOH (Figure S2c and S2d) in which the wires of conjugated polymers are embedded. Under the optimal condition of pH 12, it appears that carboxylic acids in the PCPDTBT/8BA assembly are sufficiently ionized to split off the film assembly into narrow nanowires. Meanwhile, these results indicate that the morphology of CPNWs is sensitive to changes in the pH of the aqueous solutions. The morphology might need to be stabilized through the curing reaction by

https://doi.org/10.1021/acsomega.1c05556
ACS Omega 2021, 6, 34876−34888

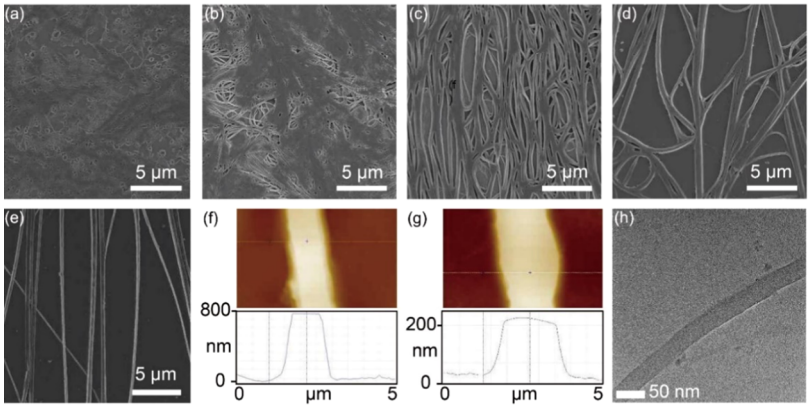

Figure 7. SEM images of CPNWs prepared by shattering film assemblies of PCPDTBT/8BA at molar mixing ratios of (a) 1:1, (b) 1:2, (c) 1:3, (d) 1:4, and (e) 1:5. AFM images of wires shattered from PCPDTBT/8BA assemblies at the 1:5 ratio (f) without and (g) with thermal annealing. (h) TEM image of a PCPDTBT/8BA nanowire shattered from PCPDTBT/8BA assembly at the 1:5 ratio after thermal annealing.

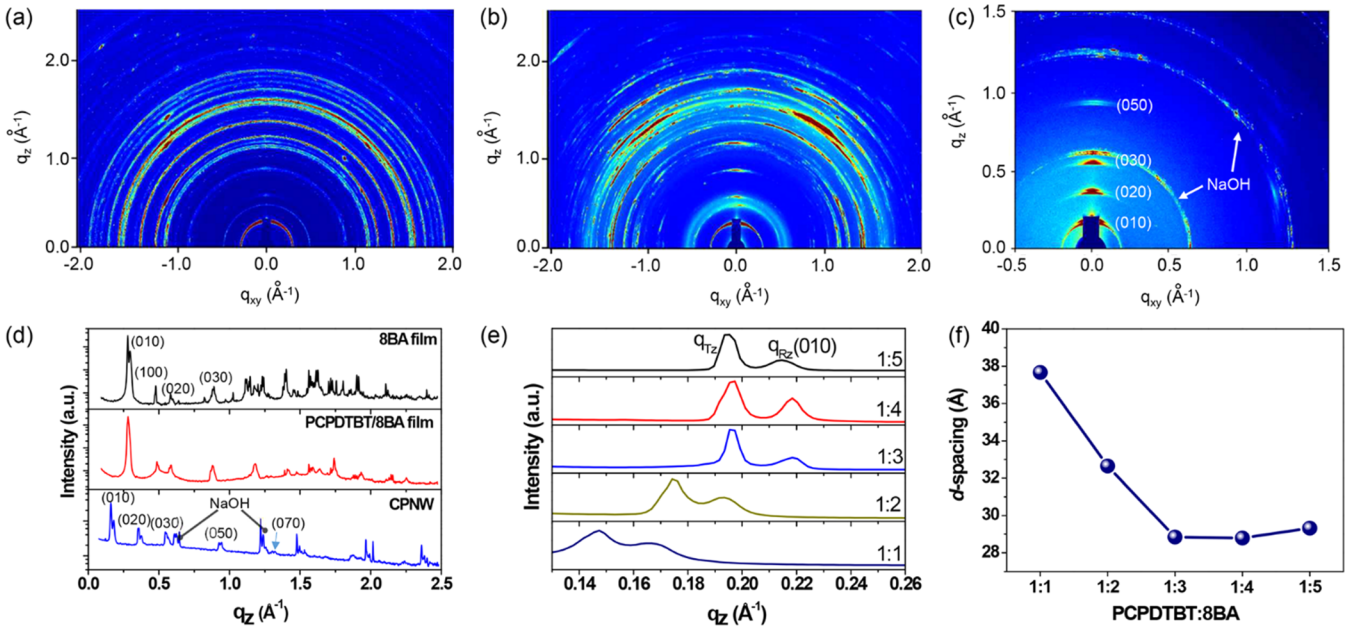

Figure 8. 2D-GIXD patterns of (a) 8BA film and (b) PCPDTBT/8BA film at a 1:5 molar mixing ratio before thermal annealing, and (c) CPNWs at a 1:5 molar mixing ratio dispersed after thermal annealing. (d) 1D line cut of 2D-GIXD of CPNWs along the out-of-plane direction. (e) Enlarged 1D patterns of the (010) plane at different molar mixing ratios. (f) *d*-Spacing of the layered structure estimated from q_{Rz} values of the (010) plane, where q_{Tz} and q_{Rz} are out-of-plane diffraction peaks by transmission and reflection, respectively.

introducing a photo-cross-linkable functional group into the chemical structure of LC alkyl benzoic acid.

To effectively assemble ethylhexyl side chains of PCPDTBT with octyls of 8BA in the crystalline structures of 8BA, it is presumed that the molar mixing ratio of PCPDTBT to 8BA should be high. As we previously reported on the assembly of PCPDTBT with a phospholipid, the molar mixing ratio of the phospholipid to PCPDTBT had to be higher than three for the successful inclusion of PCPDTBT chains into the alkyl regions of the lipid layers.[24,46] We investigated the effects of molar mixing ratios on the preparation of CPNWs by mixing PCPDTBT and 8BA at five different molar mixing ratios, from 1:1 to 1:5. Phase-separated films prepared by removing the toluene solvent were dispersed at pH 12 to facilitate the breakage of the film by ionizing the carboxylic acids at the basic condition with ultrasonication. It was clearly observed that CPNWs formed unsuccessfully at low mixing ratios, of 1:1 and 1:2 (Figure 7a,b) although the observed incompletely dispersed films at 1:1 and 1:2 lurk in curved nanowires. Separated CPNWs become straight and independent as the molar mixing ratios are increased (Figure 7c,d), presenting the complete isolation of CPNWs at the ratio of 1:5 (Figure 7e). Notably, the aspect ratio of CPNWs at 1:5 was beyond 1000 as shown in a wide view scanning electron microscopy (SEM) image (Figure S3). The formation of CPNWs at such a high aspect ratio as an aqueous dispersion occurred using both the PCPDTBT/8BA assemblies with and without thermal annealing above $T_{iso,mix}$ at the 1:5 molar mixing ratio. AFM images of PCPDTBT/8BA wires at an intermediate stage of the film dispersion process without (Figure 7f) and with (Figure 7g) thermal annealing of the films presented flat top surfaces, indicating that the wires are dispersed from crystal assemblies. Further film dispersing of the PCPDTBT/8BA assembly at the 1:5 molar mixing ratio after thermal annealing by ultrasonication could produce narrow nanowires with a

https://doi.org/10.1021/acsomega.1c05556
ACS Omega 2021, 6, 34876−34888

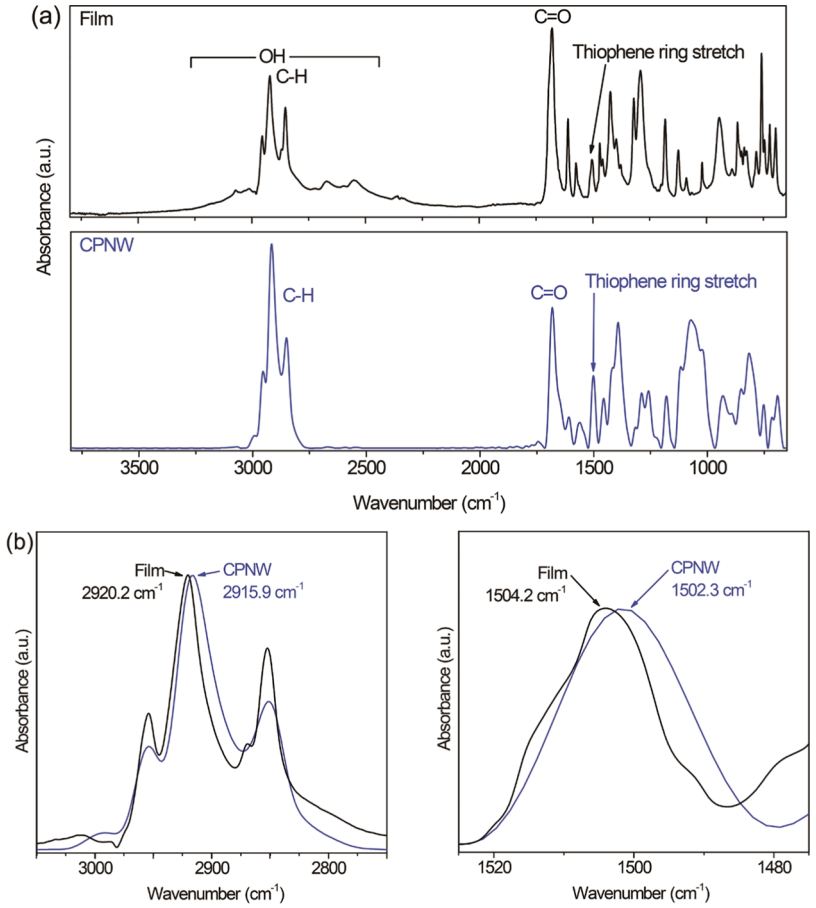

Figure 9. IR absorption spectra of (a) PCPDTBT/8BA film assembly at a 1:5 molar mixing ratio and CPNW and (b) redshifts in absorption bands of aliphatic C−H stretching and thiophene ring stretching vibration.

width of about 30 nm, as shown in a transmission electron microscopy (TEM) image (Figure 7h).

The structures of CPNWs were investigated using two-dimensional grazing-incident X-ray diffraction (2D-GIXD) in comparison to those of 8BA and PCPDTBT/8BA films assembled on silicon substrates (Figure 8). Peak positions of the (010) plane (q = 0.295 and 0.282 Å^{-1}, respectively) in the 2D-GIXD patterns of 8BA and PCPDTBT 8BA films slightly varied from peak positions in the powder patterns in Figure 6a,c (q = 0.302 and 0.302 Å^{-1}, respectively) (Figure 8a,b). Interestingly, there exist (0h0) diffractions along the out-of-plane direction, indicating an ordered layer structure of 8BA (Figure 8d). These higher-order peaks in the (0h0) diffraction did not appear in the XRD patterns of the powder samples encased in the quartz tube after scraping from the bottom of the vials (Figures 6a,c and S4). These series of (0h0) diffractions become distinct when the PCPDTBT/8BA film assembled on a silicon substrate (Figure 8b) was directly measured by GIXD, showing that preferred orientation becomes prominent on the substrate. A representative 2D-GIXD pattern of CPNWs dispersed at pH 12 from film assembly of PCPDTBT and 8BA at the 1:5 molar mixing ratio after thermal annealing, and its corresponding 1D line cut along the out-of-plane direction (Figure 8c,d, respectively), also present the series of distinct (0h0) diffractions together with diffractions by NaOH. Characteristic diffraction peaks of 8BA crystals that appear in the 2D-GIXD patterns (Figure 8a,b) are not clearly shown after dispersing the film into CPNWs except the layer peaks, indicating the disruption of the crystal structure during the dispersion process. Most notably, the position of the (010) plane in the 2D-GIXD pattern of CPNWs and its line cut was significantly shifted to q = 0.215 Å^{-1} (Figure 8c,d). The d-spacing estimated by the (010) diffraction corresponds to a thickness of one 8BA bilayer. Thus, these results indicate that the bilayer thickness of 8BA increased from about 21 Å in the powder samples to about 29 Å in CPNWs. On the other hand, enlarged 1D GIXD patterns in Figure 8e shows that the positions of (010) diffractions by transmission (q_{Tz}) and reflection beam (q_{Rz}) significantly shifted to higher q values at molar mixing ratios of 1:3, 1:4, and 1:5 than those at 1:1 and 1:2 (Figure 8e). The d-spacing values estimated using q_{Rz} decreased from 37.7 and 32.7 Å at the 1:1 and 1:2 ratios to 28.8, 28.8, and 29.3 Å at the 1:3, 1:4, and 1:5 ratios, respectively (Figure 8f). These results indicate that PCPDTBT and 8BA in CPNWs are compactly assembled into a highly ordered layer structure at molar mixing ratios beyond 1:3.

The assembly structure of CPNWs was further examined by comparing the IR spectrum of the film assembly of PCPDTBT and 8BA at the 1:5 molar mixing ratio after thermal annealing with that of CPNWs cast and dried on a wafer (Figure 9a). In the IR spectrum of the film assembly, the integration ratio of the peak of the 8BA carbonyl at 1678.8 cm^{-1} to that at 1504.2 cm^{-1} indicative of thiophene ring stretching in PCPDTBT is about 4.7:1. We could observe the peak of the thiophene stretching at 1502.3 cm^{-1} in the IR spectrum of CPNWs and

https://doi.org/10.1021/acsomega.1c05556
ACS Omega 2021, 6, 34876−34888

confirm the presence of PCPDTBT in CPNWs although other peaks of PCPDTBT are overlapped with those of 8BA. The integrated peak ratio of 8BA carbonyl to PCPDTBT thiophene stretching is 3.6:1 for CPNW, a slightly reduced value from that for film assembly. This result indicates that some 8BA molecules do not participate in CPNW formation during the film dispersion process and explains why many crystal peaks disappear except for the layering peaks and sodium-related peaks in Figure 8c. It should also be noted that no broad O−H stretching peak extending from 2500 to 3500 cm^{-1} is observed for CPNWs. This result manifests that no hydrogen bonds are present and that carboxylic acid in 8BA is in the form of sodium n-octylbenzoate.

On the other hand, by measuring any shifts in wavenumbers for C−H and thiophene vibrations, we were able to validate these improved intermolecular interactions. In enlarged spectra of aliphatic C−H stretching and thiophene ring stretching bands in Figure 9b, the asymmetric C−H stretching vibration in $-CH_3$ and $-CH_2$, and the symmetric stretching vibration in $-CH_3$ and $-CH_2$, respectively, are allocated to the IR bands of the PCPDTBT/8BA film assembly at 2954.0, 2920.2, 2869.1, and 2852.3 cm^{-1} in Figure 5a, respectively.[47] The asymmetric vibration band of $-CH_2$ was red-shifted from 2920.2 to 2915.9 cm^{-1} in the IR spectra of CPNWs produced via thermal annealing. Meanwhile, the asymmetric stretching of $-CH_3$ and symmetric stretching of CH_2 band locations stay at the same wavenumber, and the band for symmetric stretching of $-CH_3$ at 2869.1 cm^{-1} vanishes, probably incorporated in the other bands. The weakening of the C−H bond due to electron density transfer due to intermolecular interaction is indicated by the redshift of the band for the asymmetric stretching vibration in $-CH_2$, which is suggestive of alkyl chain packing. We also discovered a redshift in the thiophene ring stretching vibration from 1504.2 cm^{-1} in the film assembly to 1502.3 cm^{-1} in CPNWs, indicating greater intermolecular interaction between conjugated planes.

From the results of GIXD and IR measurements, it is credible to suggest that ionization of 8BA in the basic condition induces a lyotropic state of 8BA and that the amphiphilic 8BA can plasticize the PCPDTBT chains and further enhance the layering structure of 8BA with PCPDTBT during 8BA dissolution. The distinct enhancement of the layer peaks in Figure 8c,d compared to that of Figure 8b supports an increase in the ordered layer assembly during the dissolution process. These results also indicate that PCPDTBT chains are incorporated into the alkyl domains between the 8BA domains via alkyl chain associations, leading to an increase in the 8BA layer thickness. The most plausible molecular assembly structure is that the sodium ions coordinate with the carboxylates to form a hydrophilic layer, and the alkyl tails of 8BA bind with the alkyl side chains of PCPDTBT via hydrophobic interactions to form a hydrophobic layer, and these hydrophilic and hydrophobic layers are repeated multiple times to form a highly ordered nanowire structure.

Room-temperature electronic absorption spectra were obtained to gain information on the effect of assembly structures in CPNWs on their optical properties. In Figure 10a, representative UV−visible (UV−vis) spectra of each CPNW prepared through the dispersion process of films with and without thermal annealing show absorption maxima at 794 and 779 nm (red and blue lines in Figure 10a), respectively. Previously, the absorption spectroscopic features of PCPDTBT and its aggregates were investigated both

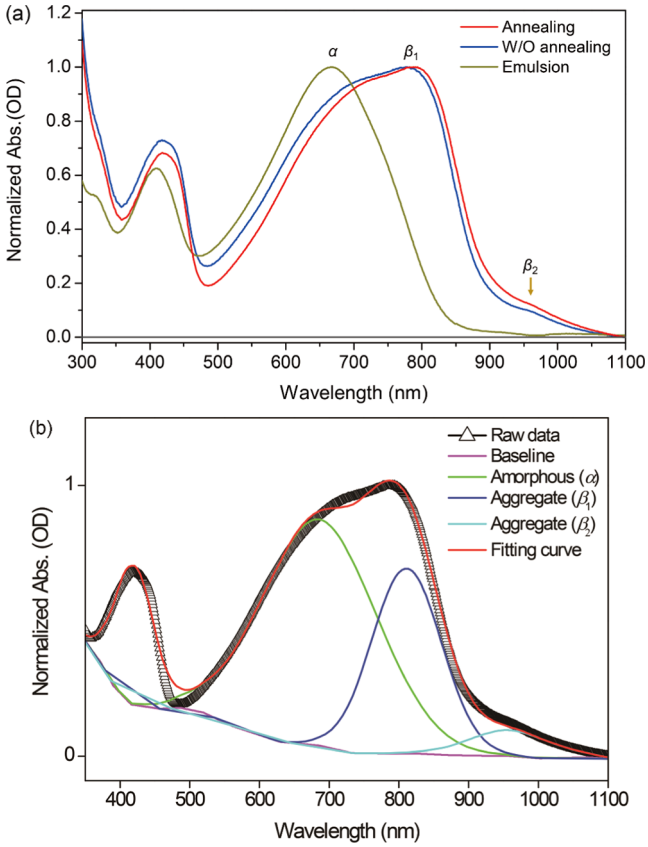

Figure 10. (a) UV−vis absorption spectra of CPNW aqueous solutions prepared with and without thermal annealing of PCPDTBT/8BA film assemblies at a 1:5 molar mixing ratio and via an emulsion process. All spectra were measured with an integrating sphere. (b) Peak deconvolution of CPNW's UV−vis absorption spectrum prepared with thermal annealing.

experimentally and theoretically.[48−51] The low-energy absorption band with a vibronic replica spanning from 600 to 900 nm has been ascribed to the S0 → S1 transition. In contrast to PCPDTBT in solution, which has the absorption peak maximum at about 710 nm, it is known that the formation of $\pi-\pi$ stacks in PCPBTBT results in a substantial redshift of 40−70 nm depending on the microstructure.[48−50] In this regard, the red-shifted absorption band of the CPNW dispersions by the film dispersion process accounts for the well-ordered microstructures and is consistent with the structural analysis results above. In particular, PCPDTBT chains form long-range π-stacking in the in-plane direction, presenting an edge-on morphology of the conjugated planes in the out-of-plane layered structure of 8BA, as shown by the diffraction of the (110), (130), and (150) planes in a 1D line cut of the 2D-GIXD pattern of the PCPDTBT/8BA film assembly along the in-plane direction (Figure S5). The interchain stacking distance estimated by the diffraction of the (150) plane is 3.8 Å, which corresponds to that of semicrystalline PCPDTBT films in the literature.[52−61] The absorption spectra show that the thermal annealing of the film assembly can cause the hydrogen bonds in the 8BA crystal structure to completely break and become a molten state, contributing to the increase of the long-range π-stacking of PCPDTBT chains. On the other hand, our control PCPDTBT dispersion, prepared by an emulsion process (green in Figure 10a) that we used in our previous report,[36] displays a

https://doi.org/10.1021/acsomega.1c05556
ACS Omega 2021, 6, 34876−34888

distinctive absorption spectrum with a band maximum at 666 nm, which is even a shorter wavelength than that of PCPDTBT single chain (~710 nm). This substantial blueshift in absorption spectrum has been noticed in a highly disordered packing of PCPDTBT that disturbs π-conjugation in a polymer backbone.[62] These results manifest the influence of the film formation and dispersion process on the enhancement of the $\pi-\pi$ stacking structure of conjugated backbones.

The CPNW's absorption spectra were further analyzed by peak deconvolution (Figure 10b). The absorption wavelength at 794 nm for CPNW prepared from the annealed film is the most red-shifted one for PCPDTBT. Even in thin films based on PCPDTBT for photovoltaic devices, the characteristic peaks are shown at around 780 nm.[51] PCPDTBT is a semicrystalline conjugated polymer with an amorphous phase (α) resulting from spaghetti-like conformation and an aggregate phase (β) resulting from strong intermolecular interactions between conjugated planes or aromatic functionalities.[50,63] Peak deconvolution shows that CPNWs have the α phase and semicrystalline polymorphs (β_1 and β_2). For CPNW produced with thermal annealing, the compositions of the α, β_1, and β_2 phases are 63.4, 31.5, and 5.1%, respectively, with center of gravity values at 685.8, 810.7, and 958.6 nm (Figure 10b). At 688.1, 806.4, and 960.1 nm, those for CPNWs without thermal annealing are 70.5, 25.7, and 3.8%, respectively. The redshift of the β_1 wavelength from 780 nm in thin-film absorption spectra of photovoltaic devices to ~810 nm in CPNW absorption spectra in our work suggests a broader delocalization due to long-range π stacking. Also, the existence of the β_2 phase implies that conjugated planes have a more organized, compact assembly structure. As revealed in a recent study of a diketopyrrolopyrrole-based polymer, the β_2 phase can be generated when intrachain disorder is reduced or interchain interaction between conjugated planes is promoted, perhaps due to a slightly smaller π-stacking distance.[64,65] Our findings suggest that lamellar layering and intermolecular alkyl chain packing during the film dispersion process cause the compact, structured assembly structure, resulting in the long-range delocalization and lower energy state.

3. CONCLUSIONS

In this study, we presented a fabrication process for nanowires of a donor−acceptor-type conjugated polymer, PCPDTBT, as an aqueous dispersion by forming its film with an amphiphilic liquid crystalline molecule, 8BA, followed by dispersing the film at a basic condition. We confirmed that the PCPDTBT and 8BA form independent phases and that the association of PCPDTBT domains with the 8BA domains decreases transition temperatures of the pristine 8BA assembly, seemingly due to a finite size effect, while the triclinic structure of the 8BA assembly is maintained. Film assemblies of PCPCDTB and 8BA could be split off into nanowires by ionization of carboxylic acids and dissolution of 8BA at a basic solution pH. GIXD and IR data showed that sodium n-octylbenzoate are compactly associated with alkyl side chains of PCPDTBT, resulting in a highly ordered layer structure of PCPDTBT and sodium n-octylbenzoate. Our experiments show that this ordered structure in CPNWs strongly enhances NIR absorption due to π−aggregates in the ordered assembly, suggesting their usefulness for light harvesting and charge transporting in aqueous-based applications. It should be noted that the morphology of nanowires is not stable with changes under ambient conditions, such as the pH of the solution, and a technology to improve the stability of the morphology of nanowires needs to be developed. Nevertheless, the absorption property and the final morphology of CPNWs prepared via the film dispersion process are truly unusual, unprecedented for PCPDTBT, showing a different domain shape, crystal habit, and optical spectrum from those polymers typically known for, and might play an important role in aqueous-based applications such as photocatalysis and biomedical applications utilizing conjugated polymers.

4. EXPERIMENTAL SECTION

4.1. Materials. PCPDTBT (M_w = 34 kDa, PDI = 2.1, MW on a repeat unit basis = 534.845 g mol^{-1}) was purchased from One Materials, Inc. (Quebec, Canada), and 8BA (M_w = 234.33 g mol^{-1}) was provided by Sigma-Aldrich (St. Louis, MO). All other chemicals were of analytical reagent grade and used as received.

4.2. Nanowire Assemblies. Phase-separated films of PCPDTBT and 8BA at five different molar mixing ratios, from 1:1 to 1:5, were prepared by dissolving both species in toluene in vials 20 mL in volume, followed by solvent removal with mild flowing of nitrogen. For example, to prepare a film at a 1:5 molar mixing ratio of PCPDTBT to 8BA, 0.200 mg (0.374 μmol on its repeat unit basis) of PCPDTBT and 0.438 mg (1.870 μmol) of 8BA were separately dissolved in 1 mL of toluene, and then both solutions were mixed in a vial and treated under ultrasonication for 5 min to completely mix both species. The toluene solvent was removed by nitrogen streaming, resulting in assembly films of PCPDTBT and 8BA on the bottom of the vials. The films were further dried in vacuum at room temperature overnight. To the vials with films on their bottom, 2 mL of pH-controlled water was added. The pH of the water was adjusted to five different values in the range 10−14, and each was then added to the vials to investigate the effect of solution pH on film shattering. The solutions were then treated under ultrasonication for 30 min with a bath-type sonicator (Branson 1510R-DTH, Branson, Newtown, CT), followed by another 30 min with a probe-type sonicator (Sonics VCX0750, Sonics & Materials, Newtown, CT) to shatter the films and obtain aqueous dispersions of CPNWs.

4.3. Characterization. The UV−vis absorption spectra of the CPNW dispersions were obtained using a UV−vis spectrometer (V-770, JASCO, Tokyo, Japan), equipped with an integrating sphere. Attenuated total reflection FT-IR spectra of 8BA, PCPDTBT, and PCPDTBT/8BA films were recorded using an FT-IR spectrometer (Nicolet 6700, Thermo Scientific, Waltham, MA). The films' phase transitions were monitored by a DSC (214 Polyma, NETZSCH Co., Ltd., Selb, Germany) with a scanning rate of 10 °C min^{-1} in a nitrogen atmosphere. Data in the second heating were used for analysis. Morphological observations of the nanostructures were conducted using a field-emission SEM (SIGMA, Carl Zeiss, Oberkochen, Germany), a high-resolution TEM (JEM3010, JEOL, Akishima, Japan), and an AFM (XE-100, PSIA, Suwon-si, South Korea). Structural analysis using powder XRD and 2D-GIXD was conducted at a synchrotron facility (6D UNIST-PAL beamline of PLS-II at Pohang Accelerator Laboratory, Pohang, Republic of Korea). The X-rays coming from the bending magnet were monochromated at 11.6 keV (wavelength: 1.0688 Å) using Si (111) double crystals and were focused at the detector position using a combination of a sagittal-type monochromator crystal and a toroidal mirror

https://doi.org/10.1021/acsomega.1c05556
ACS Omega 2021, 6, 34876−34888

system. The incidence angle of the X-ray beam was set to 0.13°, and the sample-to-detector distance was ca. 246 mm for the GIXD experiments. Temperature-dependent XRD studies were done while spinning the capillary after filling powder samples in a quartz capillary (diameter 200 μm). Scattering patterns were recorded with a 2D CCD detector (MX225-HS, Rayonix L.L.C.), and the diffraction angles were calibrated using a lanthanum hexaboride (LaB6) standard (NISTSRM 660b).

■ ASSOCIATED CONTENT

Supporting Information

The Supporting Information is available free of charge at https://pubs.acs.org/doi/10.1021/acsomega.1c05556.

Representative analysis result of XRD data based on a whole-pattern profile matching method, temperature-dependent Rietveld analysis results of XRD data, CPNWs under different basic conditions, and an optical image of the film assembly and its 1D line cut of 2D-GIXD pattern along the in-plane direction (PDF)

■ AUTHOR INFORMATION

Corresponding Authors

Tae Joo Shin − *UNIST Central Research Facilities & School of Natural Science, Ulsan National Institute of Science and Technology (UNIST), Ulsan 44919, Republic of Korea*; Email: tjshin@unist.ac.kr

Juhyun Park − *Department of Intelligent Energy and Industry, School of Chemical Engineering and Materials Science, Chung-Ang University, Seoul 06974, Republic of Korea*; orcid.org/0000-0003-1300-5743; Email: jpark@cau.ac.kr

Authors

Byoung Yun Jeon − *Department of Intelligent Energy and Industry, School of Chemical Engineering and Materials Science, Chung-Ang University, Seoul 06974, Republic of Korea*

Alemayehu Kidanemariam − *Department of Intelligent Energy and Industry, School of Chemical Engineering and Materials Science, Chung-Ang University, Seoul 06974, Republic of Korea*

Juran Noh − *Department of Materials Science and Engineering, Texas A&M University, College Station, Texas 77843, United States*

Chohee Hyun − *UNIST Central Research Facilities & School of Natural Science, Ulsan National Institute of Science and Technology (UNIST), Ulsan 44919, Republic of Korea*

Hyun Jung Mun − *UNIST Central Research Facilities & School of Natural Science, Ulsan National Institute of Science and Technology (UNIST), Ulsan 44919, Republic of Korea*

Kangho Park − *Department of Chemical and Biomolecular Engineering (BK-21 Plus) & KAIST Institute for NanoCentury, Korea Advanced Institute of Science and Technology, Daejeon 34141, Republic of Korea*

Seung-Jin Jung − *Department of Chemistry and Nanoscience, Ewha Womans University, Seoul 03760, Republic of Korea*

Yejee Jeon − *Department of Intelligent Energy and Industry, School of Chemical Engineering and Materials Science, Chung-Ang University, Seoul 06974, Republic of Korea*

Pil J. Yoo − *School of Chemical Engineering, SKKU Advanced Institute of nanotechnology (SAINT), Sungkyunkwan University, Suwon 16419, Republic of Korea*; orcid.org/0000-0002-5499-6566

JaeHong Park − *Department of Chemistry and Nanoscience, Ewha Womans University, Seoul 03760, Republic of Korea*; orcid.org/0000-0002-0509-3934

Hee-Tae Jung − *Department of Chemical and Biomolecular Engineering (BK-21 Plus) & KAIST Institute for NanoCentury, Korea Advanced Institute of Science and Technology, Daejeon 34141, Republic of Korea*; orcid.org/0000-0002-5727-6732

Complete contact information is available at: https://pubs.acs.org/10.1021/acsomega.1c05556

Author Contributions

▽B.Y.J. and A.K. equally contributed to this work. The manuscript was written through contributions of all authors and managed in overall by J.P. and T.J.S. All authors have given approval to the final version of the manuscript.

Notes

The authors declare no competing financial interest.

■ ACKNOWLEDGMENTS

This research was supported by the Chung-Ang University Graduate Scholarship in 2020, the National Research Foundation of Korea (Grant No. NRF-2019R1A2C1090512), Korea Basic Science Institute (National Research Facilities and Equipment Center) grant funded by the Ministry of Education (Grant No. NRF-2020R1A6C101B194), and the Korea Institute of Energy Technology Evaluation and Planning (KETEP) and the Ministry of Trade, Industry & Energy (MOTIE) (Grant No. 20214000000280), Republic of Korea. This work was also supported by NRF-2018R1A5A1025224. X-ray Experiments at PLS-II beamlines were supported in part by UNIST Central Research Facilities, MSIT, and POSTECH.

■ REFERENCES

(1) Moliton, A.; Hiorns, R. C. Review of electronic and optical properties of semiconducting π-conjugated polymers: applications in optoelectronics. *Polym. Int.* **2004**, *53*, 1397−1412.

(2) Guimard, N. K.; Gomez, N.; Schmidt, C. E. Conducting polymers in biomedical engineering. *Prog. Polym. Sci.* **2007**, *32*, 876−921.

(3) Park, J. Visible and near infrared light active photocatalysis based on conjugated polymers. *J. Ind. Eng. Chem.* **2017**, *51*, 27−43.

(4) Yang, D. S.; Barlóg, M.; Park, J.; Chung, K.; Shanker, A.; Sun, J.; Kang, J.; Lee, K.; Al-Hashimi, M.; Kim, J. Alignment of lyotropic liquid crystalline conjugated polymers in floating films. *ACS Omega* **2018**, *3*, 14807−14813.

(5) Wu, D.; Kaplan, M.; Ro, H. W.; Engmann, S.; Fischer, D. A.; DeLongchamp, D. M.; Richter, L. J.; Gann, E.; Thomsen, L.; McNeill, C. R.; Zhang, X. Blade coating aligned, high-performance, semiconducting-polymer transistors. *Chem. Mater.* **2018**, *30*, 1924−1936.

(6) Cho, N. G.; Shome, S.; Yu, E. S.; Shin, H. J.; Lee, B. R.; Kim, I. T.; Choi, H. Impact of chalcogenophenes on donor-acceptor copolymers for bulk heterojunction solar cells. *Macromol. Res.* **2020**, *28*, 1111−1115.

(7) Xin, H.; Yan, W.; Jenekhe, S. A. Color-stable white organic light-emitting diodes utilizing a blue-emitting electron-transport layer. *ACS Omega* **2018**, *3*, 12549−12553.

(8) Dey, A.; Kabra, D. Role of Bimolecular Exciton Kinetics in Controlling the Efficiency of Organic Light-Emitting Diodes. *ACS Appl. Mater. Interfaces* **2018**, *10*, 38287−38293.

(9) Zeng, X.; Luo, J.; Zhou, T.; Chen, T.; Zhou, X.; Wu, K.; Zou, Y.; Xie, G.; Gong, S.; Yang, C. Using ring-opening metathesis

polymerization of norbornene to construct thermally activated delayed fluorescence polymers: high-efficiency blue polymer light-emitting diodes. *Macromolecules* **2018**, *51*, 1598−1604.
(10) Günes, S.; Neugebauer, H.; Sariciftci, N. S. Conjugated polymer-based organic solar cells. *Chem. Rev.* **2007**, *107*, 1324−1338.
(11) Saito, M.; Koganezawa, T.; Osaka, I. Correlation between distribution of polymer orientation and cell structure in organic photovoltaics. *ACS. Appl. Mater. Interfaces* **2018**, *10*, 32420−32425.
(12) Cha, H.; Li, J.; Li, Y.; Kim, S.-O.; Kim, Y.-H.; Kwon, S.-K. Effects of bulk eterojunction morphology control via thermal annealing on the fill factor of anthracene-based polymer solar cells. *Macromol. Res.* **2020**, *28*, 820−825.
(13) Jiang, Y.; Pu, K. Multimodal biophotonics of semiconducting polymer nanoparticles. *Acc. Chem. Res.* **2018**, *51*, 1840−1849.
(14) Urbano, L.; Clifton, L.; Ku, H. K.; Kendall-Troughton, H.; Vandera, K.-K. A.; Matarese, B. F. E.; Abelha, T.; Li, P.; Desai, T.; Dreiss, C. A.; Barker, R. D.; Green, M. A.; Dailey, L. A.; Harvey, R. D. Influence of the surfactant structure on photoluminescent π-conjugated polymer nanoparticles: interfacial properties and protein binding. *Langmuir* **2018**, *34*, 6125−6137.
(15) Xie, C.; Lyu, Y.; Zhen, X.; Miao, Q.; Pu, K. Activatable semiconducting oligomer amphiphile for near-infrared luminescence imaging of biothiols. *ACS Appl. Bio Mater.* **2018**, *1*, 1147−1153.
(16) McQuade, D. T.; Pullen, A. E.; Swager, T. M. Conjugated polymer-based chemical sensors. *Chem. Rev.* **2000**, *100*, 2537−2574.
(17) Liu, Z.; Zhang, G.; Zhang, D. Modification of side chains of conjugated molecules and polymers for charge mobility enhancement and sensing functionality. *Acc. Chem. Res.* **2018**, *51*, 1422−1432.
(18) Inal, S.; Rivnay, J.; Suiu, A.; Malliaras, G. G.; McCulloch, L. Conjugated polymers in bioelectronics. *Acc. Chem. Res.* **2018**, *51*, 1368−1376.
(19) Pu, K.; Shuhendler, A. J.; Jokerst, J. V.; Mei, J.; Gambhir, S. S.; Bao, Z.; Rao, J. Semiconducting polymer nanoparticles as photoacoustic molecular imaging probes in living mice. *Nat. Nanotechnol.* **2014**, *9*, 233−239.
(20) Cui, L.; Rao, J. Semiconducting polymer nanoparticles as photoacoustic molecular imaging probes. *Wiley Interdiscip. Rev.: Nanomed. Nanobiotechnol.* **2016**, *9*, No. e1418.
(21) Pham, T.-T. D.; Seo, Y. H.; Lee, D.; Noh, J.; Chae, J.; Kang, E.; Park, J.; Shin, T. J.; Kim, S.; Park, J. Ordered assemblies of Fe3O4 and a donor-acceptor-type π-conjugated polymer in nanoparticles for enhanced photoacoustic and magnetic effects. *Polymer* **2019**, *161*, 205−213.
(22) Li, S.; Wang, X.; Hu, R.; Chen, H.; Li, M.; Wang, J.; Wang, Y.; Liu, L.; Lv, F.; Liang, X.-J.; Wang, S. Near-infrared (NIR)-absorbing conjugated polymer dots as highly effective photothermal materials for in vivo cancer therapy. *Chem. Mater.* **2016**, *28*, 8669−8675.
(23) Xu, L.; Cheng, L.; Wang, C.; Peng, R.; Liu, Z. Conjugated polymers for photothermal therapy of cancer. *Polym. Chem.* **2014**, *5*, 1573−1580.
(24) Yoon, J.; Kwag, J.; Shin, T. J.; Park, J.; Lee, Y. M.; Lee, Y.; Park, J.; Heo, J.; Joo, C.; Park, T. J.; Yoo, P. J.; Kim, S.; Park, J. Nanoparticles of conjugated polymers prepared from phase-separated films of phospholipids and polymers for biomedical applications. *Adv. Mater.* **2014**, *26*, 4559−4564.
(25) Muktha, B.; Madras, G.; Guru Row, T. N.; Scherf, U.; Patil, S. Conjugated polymers for photocatalysis. *J. Phys. Chem. B* **2007**, *111*, 7994−7998.
(26) Sprick, R. S.; Bai, Y.; Guilbert, A. A. Y.; Zbiri, M.; Aitchison, C. M.; Wilbraham, L.; Yan, Y.; Woods, D. J.; Zwijnenburg, M. A.; Cooper, A. I. Photocatalytic hydrogen evolution from water using fluorene and dibenzothiophene sulfone-conjugated microporous and linear polymers. *Chem. Mater.* **2019**, *31*, 305−313.
(27) Jeon, G. G.; Lee, M.; Nam, J.; Park, W.; Yang, M.; Choi, J. −H.; Yoon, D. K.; Lee, E.; Kim, B.; Kim, J. H. Simple solvent engineering for high-mobility and thermally robust conjugated polymer nanowire field-effect transistors. *ACS Appl. Mater. Interfaces* **2018**, *10*, 29824−29830.
(28) Jo, G.; Jeong, J. W.; Choi, S.; Kim, H.; Park, J.-J.; Jung, J.; Chang, M. Large-scale alignment of polymer semiconductor nanowires for efficient charge transport via controlled evaporation of confined fluids. *ACS Appl. Mater. Interfaces* **2019**, *11*, 1135−1142.
(29) Noh, J.; Jung, S.; Koo, D. G.; Kim, G.; Choi, K. S.; Park, J.; Shin, T. J.; Yang, C.; Park, J. Thienoisoindigo-based semiconductor nanowires assembled with 2-bromobenzaldehyde via both halogen and chalcogen bonding. *Sci. Rep.* **2018**, *8*, No. 14448.
(30) Ghosh, S.; Kouamé, N. A.; Ramos, L.; Remita, S.; Dazzi, A.; Deniset-Besseau, A.; Beaunier, P.; Goubard, F.; Aubert, P.-H.; Remita, H. Conducting polymer nanostructures for photocatalysis under visible light. *Nat. Mater.* **2015**, *14*, 505−511.
(31) Wei, Z.; Hu, J.; Zhu, K.; Wei, W.; Ma, X.; Zhu, Y. Self-assembled polymer phenylethnylcopper nanowires for photoelectrochemical and photocatalytic performance under visible light. *Appl. Catal., B* **2018**, *226*, 616−623.
(32) Ghosh, S.; Maiyalagan, T.; Basu, R. N. Nanostructured conducting polymers for energy applications: towards a sustainable platform. *Nanoscale* **2016**, *8*, 6921−6947.
(33) Noh, J.; Jung, S.; Kim, G.; Koo, D. G.; Choi, K. S.; Shin, T. J.; Yang, C.; Park, J. Aqueous dispersions of thienoisoindigo-based semiconductor nanorods assembled with 2-bromobenzaldehyde and a phospholipid. *J. Mol. Liq.* **2019**, *288*, No. 111046.
(34) Zang, L.; Che, Y.; Moore, J. S. One-dimensional self-assembly of planar π-conjugated molecules: adaptable building blocks for organic nanodevices. *Acc. Chem. Res.* **2008**, *41*, 1596−1608.
(35) Balakrishnan, K.; Datar, A.; Zhang, W.; Yang, X.; Naddo, T.; Huang, J.; Zuo, J.; Yen, M.; Moore, M. S.; Zang, L. Nanofibril self-assembly of an arylene ethynylene macrocycle. *J. Am. Chem. Soc.* **2006**, *128*, 6576−6577.
(36) Bae, N.; Park, H.; Yoo, P. J.; Shin, T. J.; Park, J. Nanowires of amorphous conjugated polymers prepared via a surfactant-templating process using an alkylbenzoic acid. *J. Ind. Eng. Chem.* **2017**, *51*, 172−177.
(37) Monte, M. J. S.; Almeida, A. R. R. P.; Ribeiro da Silva, M. A. V. Thermodynamic study of the sublimation of eight 4-n-alkylbenzoic acids. *J. Chem. Thermodyn.* **2004**, *36*, 385−392.
(38) Privalko, V. P.; Puchkovskaya, G. A.; Shermatov, E. N.; Yakubov, A. A. Polymorphic transitions in alkylbenzoic acids. *Mol. Cryst. Liq. Cryst.* **1985**, *126*, 289−297.
(39) Suzuki, Y.; Uta, T.; Ida, T.; Mizuno, M.; Murakami, M.; Tansho, M.; Shimizu, T. 2H and 13C NMR studies of molecular orientation and dynamics in liquid crystal 6BA. *J. Phys. Chem. Solids* **2010**, *71*, 389−393.
(40) Bakker, J. M.; Aleese, L. M.; von Helden, G.; Meijer, G. The infrared absorption spectrum of the gas phase neutral benzoic acid monomer and dimer. *J. Chem. Phys.* **2003**, *119*, 11180.
(41) Dettinger, U.; Egelhaaf, H.-J.; Brabec, C. J.; Latteyer, F.; Peisert, H.; Chassé, T. FTIR Study of the Impact of PC[60]BM on the Photodegradation of the Low Band Gap Polymer PCPDTBT under O2 Environment. *Chem. Mater.* **2015**, *27*, 2299−2308.
(42) Fischer, F. S. U.; Trefz, D.; Back, J.; Kayunkid, N.; Tornow, B.; Albrecht, S.; Yager, K. G.; Singh, G.; Karim, A.; Neher, D.; Brinkmann, M.; Ludwigs, S. Highly Crystalline films of PCPDTBT with branched side chains by solvent vapor crystallization: Influence on opto-electronic properties. *Adv. Mater.* **2015**, *27*, 1223−1228.
(43) Fischer, F. S. U.; Kayunkid, N.; Trefz, D.; Ludwigs, S.; Brinkmann, M. Structural models of poly(cyclopentadithiophene-alt-benzothiadiazole) with branched side chains: impact of a single fluorine atom on the crystal structure and polymorphism of a conjugated polymer. *Macromolecules* **2015**, *48*, 3974−3982.
(44) Kuz'mina, L. G.; Pestov, S. M.; Kochetov, A. N.; Churakov, A. V.; Lermontova, E. Kh. Molecular and crystal structure of 4-hexylbenzoic acid: Design of the mesophase. *Crystallogr. Rep.* **2010**, *55*, 786−792.
(45) Harris, D. C. *Quantitative Chemical Analysis*; 8th ed.; WH Freeman, 2010; pp AP12.
(46) Choi, Y. K.; Lee, D.; Lee, S. Y.; Shin, T. J.; Park, J.; Ahn, D. J. Conjugated polymer nanoparticles in aqueous media by assembly

https://doi.org/10.1021/acsomega.1c05556
ACS Omega 2021, 6, 34876−34888

with phospholipids via dense alkyl chain packing. *Macromolecules* **2017**, *50*, 6935−6944.
(47) Casado, J.; Pappenfus, T. M.; Mann, K. R.; Orti, E.; Viruela, P. M.; Milian, B.; Hernandez, V.; Navarret, J. T. L. Spectroscopic and theoretical study of the molecular and electronic structures of a terthiophene-based quinodimethane. *Chem. Phys. Chem.* **2004**, *5*, 529−539.
(48) Mühlbacher, D.; Scharber, M.; Morana, M.; Zhu, Z.; Waller, D.; Gaudiana, R.; Brabec, C. High photovoltaic performance of a low-bandgap polymer. *Adv. Mater.* **2006**, *18*, 2884−2889.
(49) Hwang, I.-W.; Soci, C.; Moses, D.; Zhu, Z.; Waller, D.; Gaudiana, R.; Brabec, C. J.; Heeger, A. J. Ultrafast electron transfer and decay dynamics in a small band gap bulk heterojunction material. *Adv. Mater.* **2007**, *19*, 2307−2312.
(50) Peet, J.; Kim, J. Y.; Coates, N. E.; Ma, W. L.; Moses, D.; Heeger, A. J.; Bazan, G. C. Efficiency enhancement in low-bandgap polymer solar cells by processing with alkane dithiols. *Nat. Mater.* **2007**, *6*, 497−500.
(51) Fazzi, D.; Grancini, G.; Maiuri, M.; Brida, D.; Cerullo, G.; Lanzani, G. Ultrafast internal conversion in a low band gap polymer for photovoltaics: experimental and theoretical study. *Phys. Chem. Chem. Phys.* **2012**, *14*, 6367−6374.
(52) Chen, H. Y.; Hou, J.; Hayden, A. E.; Yang, H.; Houk, K.; Yang, Y. Silicon atom substitution enhances interchain packing in a thiophene-based polymer system. *Adv. Mater.* **2010**, *22*, 371−375.
(53) Li, Y.; Chen, Y.; Liu, X.; Wang, Z.; Yang, X.; Tu, Y.; Zhu, X. Controlling blend film morphology by varying alkyl side chain in highly coplanar donor−acceptor copolymers for photovoltaic application. *Macromolecules* **2011**, *44*, 6370−6381.
(54) Murphy, A. R.; Liu, J.; Luscombe, C.; Kavulak, D.; Fréchet, J. M.; Kline, R. J.; McGehee, M. D. Synthesis, characterization, and field-effect transistor performance of carboxylate-functionalized polythiophenes with increased air stability. *Chem. Mater.* **2005**, *17*, 4892−4899.
(55) Faied, K.; Frechette, M.; Ranger, M.; Mazerolle, L.; Levesque, I.; Leclerc, M.; Chen, T.-A.; Rieke, R. D. Chromic phenomena in regioregular and nonregioregular polythiophene derivatives. *Chem. Mater.* **1995**, *7*, 1390−1396.
(56) Rughooputh, S.; Hotta, S.; Heeger, A.; Wudl, F. Chromism of soluble polythienylenes. *J. Polym. Sci., Part B: Polym. Phys.* **1987**, *25*, 1071−1078.
(57) Seo, D.; Park, J.; Shin, T. J.; Yoo, P. J.; Park, J.; Kwak, K. Bathochromic shift in absorption spectra of conjugated polymer nanoparticles with displacement along backbones. *Macromol. Res.* **2015**, *23*, 574−577.
(58) Di Nuzzo, D.; Viola, D.; Fischer, F. S. U.; Cerullo, G.; Ludwigs, S.; Da Como, E. Enhanced photogeneration of polaron pairs in neat semicrystalline donor−acceptor copolymer films via direct excitation of interchain aggregates. *J. Phys. Chem. Lett.* **2015**, *6*, 1196−1203.
(59) Kahmann, S.; Fazzi, D.; Matt, G. J.; Thiel, W.; Loi, M. A.; Brabec, C. J. Polarons in narrow band gap polymers probed over the entire infrared range: a joint experimental and theoretical investigation. *J. Phys. Chem. Lett.* **2016**, *7*, 4438−4444.
(60) Tautz, R.; Da Como, E.; Limmer, T.; Feldmann, J.; Egelhaaf, H.-J.; von Hauff, E.; Lemaur, V.; Beljonne, D.; Yilmaz, S.; Dumsch, I.; Allard, S.; Scherf, U. Structural correlations in the generation of polaron pairs in low-bandgap polymers for photovoltaics. *Nat. Commun.* **2012**, *3*, No. 970.
(61) Etzold, F.; Howard, I. A.; Forler, N.; Cho, D. M.; Meister, M.; Mangold, H.; Shu, J.; Hansen, M. R.; Müllen, K.; Laquai, F. The effect of solvent additives on morphology and excited-state dynamics in PCPDTBT: PCBM photovoltaic blends. *J. Am. Chem. Soc.* **2012**, *134*, 10569−10583.
(62) Abelha, T. F.; Neumann, P. R.; Holthof, J.; Dreiss, C. A.; Alexander, C.; Green, M.; Dailey, L. A. Low molecular weight PEG−PLGA polymers provide a superior matrix for conjugated polymer nanoparticles in terms of physicochemical properties, biocompatibility and optical/photoacoustic performance. *J. Mater. Chem. B* **2019**, *7*, 5115−5124.
(63) Steyrleuthner, R.; Schubert, M.; Howard, I.; Klaumunzer, B.; Shilling, K.; Chen, Z.; Saalfrank, P.; Laquai, F.; Facchetti, A.; Neher, D. Aggregation in a high-mobility n-type low-bandgap copolymer with implications on semicrystalline morphology. *J. Am. Chem. Soc.* **2012**, *134*, 18303−18317.
(64) Li, M.; Balawi, A. H.; Leenaers, P. J.; Ning, L.; Heintges, G. H. L.; Marszalek, T.; et al. Impact of polymorphism on the optoelectronic properties of a low-bandgap semiconducting polymer. *Nat. Commun.* **2019**, *10*, No. 2867.
(65) Li, M.; Leenaers, P. J.; Wienk, M. M.; Janssen, R. A. J. The effect of alkyl side chain length on the formation of two semicrystalline phases in low band gap conjugated polymers. *J. Mater. Chem. C* **2020**, *8*, 5856−5867.

https://doi.org/10.1021/acsomega.1c05556
ACS Omega 2021, 6, 34876−34888